Graphical Abstract

Maximum spreading of an impacting drop

Martin Wörner

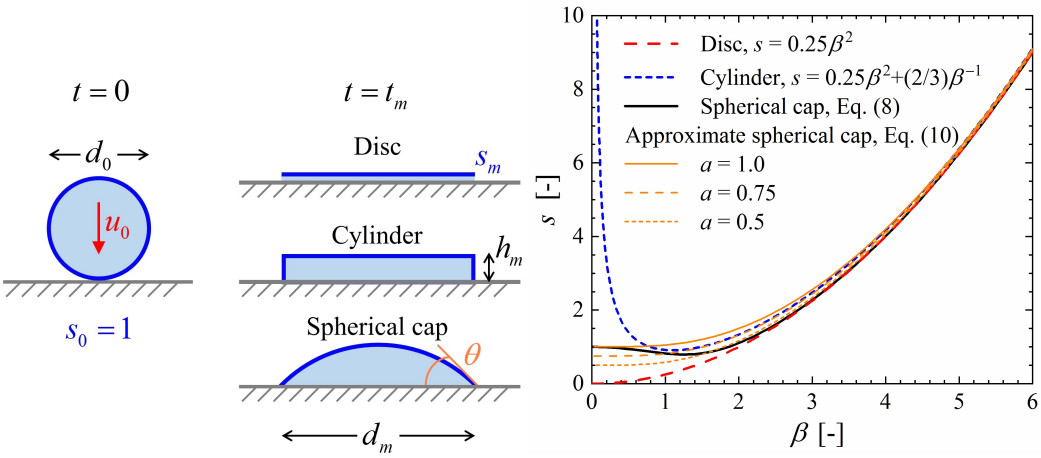

Highlights

Maximum spreading of an impacting drop

Martin Wörner

- Proposal of two novel closures for the drop energy balance
- Approximate spherical cap model for drop deformation
- Dissipation model upon maximum spread relative to total dissipation
- Explicit model for maximum spread factor including three scaling laws

Maximum spreading of an impacting drop

Martin Wörner

[a]*Karlsruhe Institute of Technology (KIT) Institute of Catalyis Research and Technology Engesserstr. 20 76131 Karlsruhe Germany*

Abstract

The maximum diameter of a drop impacting on a flat solid surface is studied theoretically assuming axi-symmetric spreading without splashing. The energy balance between the initial state of the drop (sphere diameter d_0) and that a maximum spread (contact diameter d_m) is closed by two novel concepts. For the gas-liquid surface area, an approximate spherical cap model is proposed. Energy loss by viscous dissipation is related to the total energy dissipation when the drop has come to rest. The fractional dissipation upon maximum spread is modelled as a function of an impact parameter (P) that combines the power laws of the capillary and viscous regimes depending on a regime discrimination parameter (A). Exponents of the Weber (We) and Reynolds (Re) numbers in $P = WeRe^{-2/5}$ are determined by asymptotic analysis. The parameter A is determined from experimental data as a function of the advancing contact angle (θ_a). In this way, an explicit model for the maximum spread factor ($\beta_m = d_m/d_0$) is proposed which includes the scaling laws $\beta_m \sim We^{1/2}$, $\beta_m \sim We^{1/4}$ and $\beta_m \sim Re^{1/5}$ and is in good agreement with experimental data for wide ranges of We, Re and θ_a.

Keywords: drop impact, maximum spread factor, energy balance

1. Introduction

Drop collision with a wall is an important element of various industrial spray processes including spray cooling (Liang and Mudawar, 2017; Breitenbach et al., 2018), spray coating (Ye and Domnick, 2017), combustion (Moreira et al., 2010) and ink-jet printing (Castrejon-Pita et al., 2013) to name a few. The state of fluid dynamic knowledge is summarised in various reviews (Rein, 1993; Yarin, 2006; German and Bertola, 2009; Marengo et al.,

2011; Josserand and Thoroddsen, 2016; Fang et al., 2022). The main dimensionless parameters governing the dynamics of drop spreading on a dry wall are the impact Weber number ($We = \rho d_0 u_0^2/\sigma$) and the impact Reynolds number ($Re = \rho d_0 u_0/\mu$). Here, u_0 and d_0 are the impact velocity and initial drop diameter while ρ, μ and σ indicate the density, dynamic viscosity and surface tension of the liquid, respectively.

In addition to the above parameters, the drop impact dynamics depends on the wetting properties of the solid. The wettability of a surface by a liquid is commonly characterised by the contact angle (θ), where different definitions exist (Marmur et al., 2017). For an ideal smooth and chemically homogeneous surface, the equilibrium contact angle (θ_e) is uniquely defined by the single minimum of the Gibbs free energy (the change in the surface energy of the solid due to wetting). In practice, any solid surface is heterogeneous at small scales because of either topographic roughness or chemical defects. In experiments then an apparent (global) contact angle is routinely obtained, which is the contact angle measured at a length scale much bigger than the surface structure or variations in its chemical composition (Butt et al., 2022). For real surfaces, the Gibbs energy possesses multiple minima points which correspond to several possible metastable states of a static drop (Kung et al., 2019). The contact angle of a static drop (θ_s) is therefore not unique but within a range $\theta_r \leq \theta_s \leq \theta_a$. Here, θ_r and θ_a denote the receding/advancing contact angles which are the lowest/highest metastable contact angles that can be measured (e.g. by decreasing or increasing the volume of a drop). The metastable static states thus give rise to contact angle hysteresis $\Delta\theta = \theta_a - \theta_r \geq 0$. For water, $\Delta\theta$ is typically larger than 10°, even on seemingly smooth and homogeneous rigid surfaces (Butt et al., 2022). For a contact line that is not static but moving, the dynamic contact angle (θ_d) is affected by the velocity of the flow due to viscous effects. Hydrodynamic theories of wetting relate the deviation of θ_d from the equilibrium contact angle to the capillary number (Voinov, 1976; Cox, 1986).

Of great interest for technical applications is the maximum spread factor $\beta_m = d_m/d_0$ where d_m is the maximum spread diameter of the drop. Approaches for predicting β_m can be classified in scaling laws (Collings et al., 1990; Clanet et al., 2004; Fedorchenko et al., 2005), empirical correlations (Asai et al., 1993; Scheller and Bousfield, 1995; Bayer and Megaridis, 2006) and models based on a momentum balance (Clanet et al., 2004; Roisman, 2009; Gordillo et al., 2019) or an energy balance (Engel, 1955; Ford and Furmidge, 1967; Madejski, 1976; Chandra and Avedisian, 1991; Park et al., 2003;

Yonemoto and Kunugi, 2017). The latter approach established a balance between the kinetic and surface energies before impact and at maximum spread while accounting for dissipation.

For the *inviscid* (or capillary) regime (limit $Re \to \infty$), the scaling law $\beta_m \sim We^{1/2}$ is obtained by assuming that initial kinetic energy is completely converted into surface at maximum spread (Collings et al., 1990; Bennett and Poulikakos, 1993). This scaling was experimentally confirmed by Laan et al. (2014) who studied the impact of four different liquids (among them water and blood) with different viscosity on five different surfaces ($20° \leq \theta_s \leq 90°$). Experiments by Clanet et al. (2004) on the impact of water droplets on a strongly water-repellent surface ($\theta_e = 170°$) show in contrast a scaling $\beta_m \sim We^{1/4}$, which is explained by a mass balance argument using the impact capillary length.

In the *viscous* regime it is assumed that most of the initial kinetic energy has been dissipated upon maximum spread. Dissipation has been proposed to scale as $W_m \sim \mu(u_0/h_m)d_0d_m^2$ (Chandra and Avedisian, 1991) or $W_m \sim \mu(u_0/h_m)d_m^3$ (Clanet et al., 2004), where h_m is the droplet height at maximum spread. Together with volume conservation ($h_m d_m^2 \sim d_0^3$) this yields $\beta_m \sim Re^{1/4}$ (Chandra and Avedisian, 1991) and $\beta_m \sim Re^{1/5}$ (Clanet et al., 2004), respectively. The latter scaling has been observed in various experiments (Madejski, 1976; Fedorchenko et al., 2005; Eggers et al., 2010).

To distinguish between the viscous and the capillary regime, an impact parameter $P = WeRe^{-4/5}$ was proposed by Clanet et al. (2004) which was revised to $P = WeRe^{-2/5}$ by Eggers et al. (2010). Since most of the scaling models were developed for a limited range of We and Re, they cannot be applied as a general model for a broader range of the impact regime (Marengo et al., 2011). Universal models based on rescaling combine one inviscid regime where $\beta_m \sim We^n$ with either $n = 0.5$ (Laan et al., 2014; Lee et al., 2016b) or $n = 0.25$ (Wang et al., 2022) with the viscous regime $\beta_m \sim Re^{1/5}$ using an approximation function that provides a smooth cross-over between both regimes.

For high viscosity liquids, the contribution of viscous dissipation is important and models based on an energy balance rather than a momentum balance are more suitable (Eggers et al., 2010). While the initial kinetic and surface energies in energy balance approaches from literature are always identical, models differ in approximation of gas-liquid surface energy at maximum spread and dissipation upon maximum spread. Variation in the dissipation arise from different assumptions on the time scale and the velocity profile in

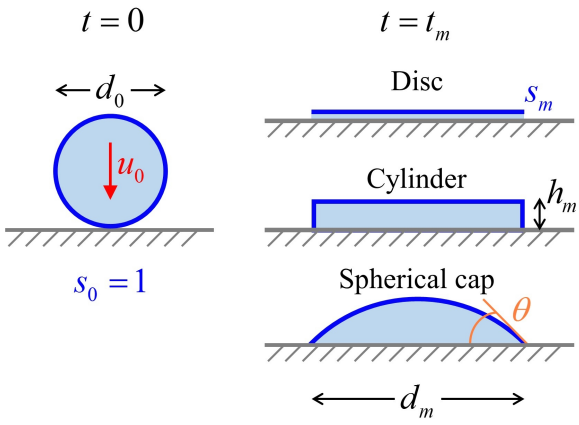

Figure 1: Sketch of initial drop at the moment of impact (left) and models for drop shape at maximum spread (right). The variables s_0 and s_m denote the normalised gas-liquid interfacial area before impact and at maximum spreading, respectively.

the spreading film. Differences in gas-liquid surface energy arise on assumptions of the droplet shape at the maximum spread, which is often considered as a cylindrical disc with negligible height (Ford and Furmidge, 1967), a flat cylinder with finite height (Mao et al., 1997) or a spherical cap (truncated sphere), see Fig. 1. The cylinder model was found to be suitable for drop impact with small values of the Ohnesorge number ($Oh = \sqrt{We}/Re < 0.002$), whereas the spherical cap model is appropriate when Oh is high (Kim and Chun, 2001). Further differences in surface energy arise from the choice of the characteristic contact angle. Some authors argue in favour of the equilibrium contact angle θ_e (Bennett and Poulikakos, 1993; Mao et al., 1997; Park et al., 2003) while others propose the advancing contact angle θ_a (Chandra and Avedisian, 1991; Pasandideh-Fard et al., 1996; Du et al., 2021) or the dynamic contact angle θ_d (Vadillo et al., 2009).

The diverse impact dynamics of drops make formulating a general prediction model, valid over large ranges of We, Re and θ difficult. Accordingly, the range of applicability of existing models is often limited. The cubic equation for β_m proposed by Mao et al. (1997) e.g. predicts negative or imaginary numbers for large values of θ (Park et al., 2003). A comprehensive overview on historical models or correlations used to predict the maximum spreading factor is provided in Table S1 of Liang et al. (2019). In particular missing so far is a mechanistic model for maximum spread which includes all experimentally observed scaling regimes where $\beta_m \sim (We^{1/4}, We^{1/2}, Re^{1/5})$.

In this work, significant progress in development of an universal model for β_m based on an energy balance instead of rescaling is reported. The study is restricted to the normal impact of a single spherical drop consisting of a viscous liquid ($\mu > 0$) on a dry, smooth, chemically homogeneous and partially wetting rigid solid surface under isothermal conditions. In addition it is assumed that the initial kinetic energy is sufficiently low so that the spreading is completely axi-symmetric, the advancing lamella stays in contact with the solid surface, and no fragmentation into secondary droplets (splashing) or breakup during receding occurs. The splashing threshold depends on wettability and viscosity and we refer to Almohammadi and Amirfazli (2019) for a general empirical relationship that captures available experimental data. Novelties proposed in the present paper are as follows: (i) a drop deformation model which improves currents models for hydrophobic substrates, (ii) a dissipation model which accounts for the proper upper physical bound for energy dissipation, and (iii) an explicit model for the maximum spread factor which includes all three scaling laws with respect to We and Re and is in reasonable agreement with experimental data from literature.

2. General energy balance

In the present energy balance approach, any influence of the air surrounding the droplet is neglected as the gas viscosity and density are usually orders of magnitude smaller than the liquid viscosity and density, respectively. Since gravitational potential energy accounts typically only for less than 2% of total initial energy, it is neglected as well. This assumption is reasonable for drops whose diameter is below the capillary length $\sqrt{\sigma/(\rho g)}$ which is about 2.7 mm for water. Thus, we deal with kinetic energy (E_k) and surface energy (E_s) only. The energy balance between the initial energy of the drop at time $t = 0$ and the energy at time $t > 0$ is

$$E_{s,0} + E_{k,0} = E_s(t) + E_k(t) + W(t), \tag{1}$$

where $W(t) \geq 0$ denotes the energy loss by dissipation upon time t.

When a falling drop approaches a solid surface perpendicularly, a dimple forms at its bottom prior to impact due to the cushioning air layer thereby transforming a point contact into one along a ring, with a thin disk of air entrapped. The air-disk contracts rapidly into a small central bubble on the substrate, to minimise surface energy (Josserand and Thoroddsen, 2016).

Similar to other energy balance studies we assume here instead that the drop is spherical (diameter d_0, gas-liquid surface area $S_0 = \pi d_0^2$) and in point contact with the surface at time $t = 0$. We furthermore assume that all the liquid has identical downward velocity velocity u_0 resulting in the initial kinetic energy $E_{k,0} = \pi \rho_L u_0^2 d_0^3/12$. Kinetic energy at time $t > 0$ is related to the initial kinetic energy as $E_k(t) = C_k(t) E_{k,0}$. Normalising Eq. (1) by the initial gas-liquid surface energy, σS_0, yields

$$\frac{E_{s,0} - E_s(t)}{\sigma S_0} + (1 - C_k(t)) \frac{We}{12} = \frac{W(t)}{\sigma S_0}. \tag{2}$$

For $We = 12$, the drops initial kinetic and gas-liquid surface energies are equal. With definition of the reduced Weber number $We_r = We/12$, the initial kinetic energy thus dominates for $We_r > 1$ while the initial gas-liquid interfacial energy dominates for $We_r < 1$ (Zhang and Zhang, 2019).

The initial surface energy is $E_{s,0} = \sigma S_0 + \gamma_{gs} A_{gs,0}$ where γ_{gs} is the gas-solid surface energy and $A_{gs,0}$ the area of the initially dry spatially extended solid surface. The surface energy at time t is

$$E_s(t) = \sigma S(t) + \gamma_{ls} A_{ls}(t) + \gamma_{gs}[A_{gs,0} - A_{ls}(t)]. \tag{3}$$

Here, $S(t)$ is the area of the gas-liquid interface, $A_{ls}(t)$ is the wetted surface area and γ_{ls} is the liquid-solid surface energy. Because the values of γ_{gs} and γ_{ls} cannot be measured independently, Young's equation $\gamma_{gs} - \gamma_{ls} = \sigma \cos\theta$ is commonly used to relate their difference to the contact angle $\theta \in (0, \pi)$. We neglect any gas that may be entrapped by the drop and assume that the wetted surface is circular in shape with instantaneous contact diameter $d(t)$ so that $A_{ls}(t) = \pi d^2(t)/4$. With the instantaneous spreading factor $\beta(t) = d(t)/d_0$ and the notations $s(t) = S(t)/S_0$ and $w(t) = W(t)/(\sigma S_0)$ the energy balance in Eq. (2) can be expressed as

$$1 - s(t) + 0.25 \cos(\theta) \beta^2(t) + (1 - C_k(t))\ We_r = w(t). \tag{4}$$

Equation (4) represents the non-dimensional energy balance for time $t > 0$.

Here, we are interested in the maximum spread factor $\beta_m = \beta(t_m) = d_m/d_0$, where t_m denotes the time of maximum spreading and $d_m = d(t_m)$. It should be noted that with the present definitions, β_m characterises the maximum diameter of the wetted surface area, which may differ from the maximum drop dimension observed laterally or from above, depending on the contact angle at maximum spread. The kinetic energy at maximum spread,

$E_k(t_m)$, may be not negligible for impact on free-slip surfaces or when a circular flow occurs in the rim (Wildeman et al., 2016; Lin et al., 2022). For impact on no-slip surfaces as considered here, numerical simulations show that $E_k(t_m)$ is typically less than 5% of the total initial energy (Lee et al., 2016a; Zhang et al., 2021) but can be much higher for drops bouncing from hydrophobic surfaces (Samkhaniani et al., 2021). Here we set $C_k(t_m) = 0$ and thus neglect remaining kinetic energy at maximum spreading, similar to most other energy balance approaches. With this assumption, Eq. (4) yields

$$1 + We_r - s_m + 0.25\beta_m^2 \cos\theta = w_m, \tag{5}$$

where all local instantaneous fluid dynamics from the begin of the impact process until maximum spread are integrally accumulated in the dissipation term w_m. To derive a relation for β_m from the energy balance (5) models for s_m and w_m are required. In literature, most often one of two different shape models for $s_m = s_m(\beta_m)$ is used, whereas the number of dissipation models of the form $w_m = w_m(\beta_m, We, Re)$ is much larger.

3. New concepts for closure of the energy balance

In this Section, novel concepts for s_m and w_m are proposed for closure of Eq. (5) in order to derive a model for β_m.

3.1. Drop deformation and gas-liquid surface area at maximum spread

Solution of Eq. (4) requires a model for $s(t)$, i.e. the normalised gas-liquid surface area at time $t > 0$. This area is closely related to drop deformation during impact, which can be quite complex (Renardy et al., 2003; Lee et al., 2016a; Wildeman et al., 2016). Modelling drop shape during impact requires a drop deformation model, which means that during spreading the droplet can change its shape depending on $\beta(t)$ but not its volume. For high We or for liquids with low viscosity, drop deformation is significant resulting in large values of β_m. The drop typically takes the shape of a thin disc-shaped liquid layer (called lamella) with or without a rim. This shape can be modelled by a disc with negligible height where $s_{\mathrm{disc}}(\beta) = \beta^2/4$. For a cylindrical drop with uniform thickness and finite lateral area, the normalised gas-liquid surface area is obtained by a mass balance as $s_{\mathrm{cyl}}(\beta) = \beta^2/4 + 2/(3\beta)$.

For estimating s_m, the disc model was introduced by Ford and Furmidge (1967) and is used e.g. in Collings et al. (1990), Chandra and Avedisian

(1991) and Pasandideh-Fard et al. (1996). The cylinder model for s_m was introduced by Mao et al. (1997) and is widely used since then (Roisman et al., 2002; Ukiwe and Kwok, 2005; Budakli, 2021; Du et al., 2021; Zhang et al., 2021; Aksoy et al., 2022). More advanced shape models account for the additional gas-liquid area of a lamella with a rim. The relative size of the rim was proposed to depend on an adjustable parameter that is a function of viscosity (Attané et al., 2007), on the contact angle (Gao and Li, 2014) or on a thickness parameter that is a function of We (Wang et al., 2019). Willis and Orme (2003) theoretically analysed for the case of binary drop collision the total surface area on a torus (the extreme case with rim) and pancake (the extreme case without rim) with the same volume and maximal diameter and showed trivial difference between the cases.

For low We or liquids with high viscosity, values of β_m are lower and drop deformations are similar in shape to a spherical cap (sc), as assumed by Park et al. (2003) and Li et al. (2010). In another approach, Yonemoto and Kunugi (2017) computed the gas-liquid surface at maximum spread as the harmonic average of the surfaces of a spherical cap and a disc. In a recent experimental study on the effect of liquid viscosity, Qin et al. (2019) stated that the difficulty of establishing a predicting model for droplet spreading below $We \approx 30$ roots in the absence of an asymptotically accurate model for droplet shape. In the following, a drop deformation model is proposed which is suitable for low and for high values of We.

For a spherical cap, the normalised area of the curved surface is

$$s_{\mathrm{sc}}(\theta) = \sqrt[3]{\frac{2}{(2+\cos\theta)^2(1-\cos\theta)}} \tag{6}$$

while the spreading factor is

$$\beta_{\mathrm{sc}}(\theta) = \sqrt[3]{\frac{4\sin^3\theta}{(2+\cos\theta)(1-\cos\theta)^2}}. \tag{7}$$

A relation between the normalised curved surface area and the spreading factor of a spherical cap seems to be missing in literature. In the Appendix, the following relationship is derived

$$s_{\mathrm{sc}}(\beta) = \frac{\sqrt[3]{\beta^6 + 8\sqrt{\beta^6+16}+32} - \beta^2}{4} + \frac{\beta^4}{4\sqrt[3]{\beta^6 + 8\sqrt{\beta^6+16}+32}}. \tag{8}$$

This non-monotonic relation is displayed in Fig. 2. The local minimum is obtained for $\beta = \sqrt[3]{2} \approx 1.26$ which corresponds by Eq. (7) to $\theta = \pi/2$. For $0 \leq \beta \leq \sqrt[4]{12} \approx 1.86$ it is $1/\sqrt[3]{2} \leq s_{\mathrm{sc}} \leq 1$ and the relation $s_{\mathrm{sc}}(\beta)$ is not unique as the same value for s_{sc} is obtained by two different values of β.

Introducing $s_m = s_{\mathrm{sc}}(\beta_m)$ according to Eq. (8) in the energy balance (5) will result in a rather complicated implicit equation for β_m. Here, we are interested in a maximum spread model that is explicit in β_m. To this end we introduce the approximation

$$\beta^6 + 8\sqrt{\beta^6 + 16} + 32 \approx (\beta^2 + 4a)^3 \tag{9}$$

where $0 \leq a \leq 1$. Inserting approximation (9) into Eq. (8) yields the new approximate spherical cap (asc) deformation model

$$s_{\mathrm{asc}}(\beta, a) = a + \frac{1}{4}\frac{\beta^4}{\beta^2 + 4a}, \tag{10}$$

where a defines the value of s_{asc} for $\beta = 0$. For $a = 0$, the model yields the disc model.

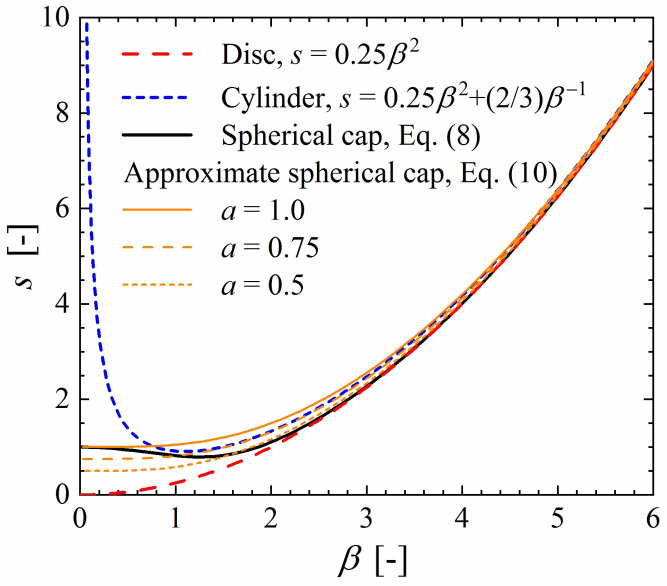

Figure 2: Normalised gas-liquid surface area (s) as function of spreading factor (β). Comparison of disc model, cylinder model, spherical cap model and approximate spherical cap model (with three different values of parameter a).

Figure 2 compares the normalised gas-liquid surface area as function of spread factor β for the different models. For $\beta > 4$ all curves overlap almost. The differences increase with decrease of β. For $\beta \to 0$ it is $s_{\mathrm{disc}} \to 0$ and $s_{\mathrm{cyl}} \to \infty$. As both shape models are not compatible with the initial state $s_0 = 1$, they are (in contrast to the sc model) unsuited to describe the drop deformation during the entire impact process. In contrast to s_{sc}, s_{asc} is monotonic in β. For $a = 0.5$ and $\beta > 1.5$, s_{asc} is in good agreement with s_{sc}. For $a = 0.75$ and $\beta > 1.5$, s_{asc} is in good agreement with s_{cyl}. For $a = 1$ and $\beta < 0.5$, s_{asc} is in good agreement with Eq. (8) and only the choice $a = 1$ ensures $s_{\mathrm{asc}} \to s_{\mathrm{sc}}$ in the limit $\beta \to 0$.

3.2. Modelling of dissipation upon maximum spread

The second difficulty in the energy balance approach is the modelling of normalised accumulative dissipation upon maximum spreading w_m. During the spreading of a liquid film, several types of dissipative processes can occur at different locations such as the wedge of fluid behind the contact line, the close vicinity of the contact line or in the precursor film (de Gennes, 1985). For drop impact, different dissipation mechanisms may dominate depending on Weber number. At sufficiently high We, dissipation within the viscous boundary layer that forms near the solid surface during the spreading process is often assumed to be dominant. The energy dissipated in the viscous boundary layer can be accounted for only if the flow in the spreading drop is known. For inertia dominated drop collisions, Roisman (2009) obtained an analytical self-similar solution for the viscous flow in the spreading drop which satisfies the full Navier–Stokes equations. In the context of the energy balance approach, Chandra and Avedisian (1991) proposed the first mechanistic model for the dissipation term. Since then, many models have been proposed where dissipation is expressed as power of β_m with different exponents ranging typically from 2 to 5. In combination with the disc or cylinder approximation for drop shape this results in maximum spread models of very different form that are usually implicit in β_m, see e.g. Aksoy et al. (2022) for an overview.

It is quite obvious that there exists an upper bound for the energy that can be dissipated during the entire impact process. Current models for dissipation from literature do, however, not account for the proper upper physical bound. Under the assumption that there is no fragmentation, the total dissipation (W_∞) can be evaluated from the energy balance Eq. (4) for terminal

time t_∞. Since the terminal kinetic energy is zero $C_k(t_\infty) = 0$ it follows

$$w_\infty = 1 + We_r - (s_\infty - 0.25\beta_\infty^2 \cos\theta), \tag{11}$$

where $w_\infty = W_\infty/(\sigma S_0)$. On the right hand side of this non-dimensional equation, the first two terms denote initial surface and kinetic energy while the terms in the bracket represent the terminal surface energy. The upper bound for dissipation is thus given by the difference between the total initial energy and the terminal surface energy. Energy balance models for β_m in literature do not consider the terminal surface energy of the drop so far. Its importance is, however, highlighted by the rescaling model of Lee et al. (2016b) where the capillary energy at zero impact velocity is included in the maximum spreading model.

As mentioned before, in energy balance approaches in literature dissipation upon maximum spread (W_m) is commonly expressed as power of β_m, with normalised dissipation upon maximum spread $w_m = W_m/(\sigma S_0)$ depending additionally on We and Re (Madejski, 1976; Chandra and Avedisian, 1991; Pasandideh-Fard et al., 1996; Mao et al., 1997; Wildeman et al., 2016). The author is not aware on any model for W_m that is a function of θ. Any dependence of W_m on wettability can therefore only be implicit and hidden in β_m. For a dissipation model where $w_m = w_m(\beta_m, We, Re)$ it follows

$$\frac{w_m}{w_\infty} = \frac{w_m(\beta_m, We, Re)}{1 + We_r - s_\infty(\beta_\infty, \theta) + 0.25\beta_\infty^2 \cos\theta}. \tag{12}$$

Physically, the ratio on the left hand side should be in the range $0 \leq w_m/w_\infty \leq 1$. On the right hand side of Eq. (12), the numerator is a direct function of Re but not of θ while the denominator is a direct function of θ but not of Re. Due to this discrepancy, common literature models for W_m will hardly meet the restriction $0 \leq W_m \leq W_\infty$ in general. To avoid this inconsistency and to account for the terminal surface energy, we propose to model the dissipation upon maximum spread as $w_m = f_w w_\infty$ where w_∞ is given by Eq. (11) and f_w is a function that describes relative dissipation upon maximum spread and satisfies $0 \leq f_w \leq 1$. With this restriction on the range of f_w, the proposed model automatically ensures $0 \leq W_m \leq W_\infty$.

To transfer the energy balance into a relation that is explicit in β_m, the function f_w will be modelled here independent on β_m. While this may seem to be a strong assumption, it is actually not. Since $\beta_m = \beta_m(We, Re, \theta)$ any function $f_w = f_w(\beta_m)$ can be rewritten as $f_w = f_w(We, Re, \theta)$.

4. Model for maximum spread during drop impact

The general model is obtained by inserting the deformation model for s_m given by Eq. (10) and the dissipation model $w_m = f_w w_\infty$ into the energy balance (5). This yields

$$\frac{1}{4}\frac{\beta_m^4}{\beta_m^2+4a} - \frac{\cos\theta}{4}\beta_m^2 - \underbrace{(1-a+We_r-f_w w_\infty)}_{=Q} = 0, \tag{13}$$

where the sum of the four terms in the brackets is denoted by Q for the sake of brevity. So far, the latter equation is unclosed in a and $f_w w_\infty$. For $a = 0$ (the disc model) and $\theta = \theta_a$ two well known literature models for maximum spreading can be recovered. For $f_w w_\infty = 3\,We Re^{-1}\beta_m^4/8$ equation (13) reduces to the model of Chandra and Avedisian (1991) while for $f_w w_\infty = We Re^{-0.5}\beta_m^2/3$ the model of Pasandideh-Fard et al. (1996) is obtained. Here, we model f_w and w_∞ independently and assume that f_w is no direct function of β_m so that Eq. (13) results is a quadratic equation for β_m^2.

The determination of the total energy dissipation w_∞ via Eq. (11) requires knowledge of the terminal drop shape when the drop has come to rest. Here, the terminal drop shape is taken as a spherical cap so that

$$\begin{aligned} w_\infty &= \underbrace{1 - s_{sc} + 0.25\beta_{sc}^2\cos\theta}_{e_{\Delta s}} + We_r \\ &= \underbrace{1 - \sqrt[3]{0.25(2+\cos\theta)(1-\cos\theta)^2}}_{e_{\Delta s}} + We_r, \end{aligned} \tag{14}$$

where we used Eq. (6) and Eq. (7). The term $e_{\Delta s}(\theta)$ expresses the difference between initial and terminal surface energy, normalised by σS_0. As θ increases from 0 to π, $e_{\Delta s}$ decreases monotonically from 1 to 0. The value $e_{\Delta s} = 0$ reflects that the initial and terminal surface energies become identical in the limit $\theta \to \pi$ as the drop is in both cases in point contact with the surface. For $We_r \gg 1$ or $\theta \to \pi$, the term $e_{\Delta s}$ can be neglected so that $w_\infty \approx We_r$.

Equation (13) has four real roots for $a > 0$, from which only the following is relevant here

$$\beta_m = \sqrt{\frac{2(Q+a\cos\theta) + 2\sqrt{(Q+a\cos\theta)^2 + 4aQ(1-\cos\theta)}}{1-\cos\theta}}. \tag{15}$$

The term in the denominator shows the prominent role of surface wettability, as recently highlighted by Wang et al. (2022). The condition $\beta_m > 0$ requires $Q > 0$, where Q is defined in Eq. (13). The minimum of Q is obtained for $f_w = 1$. In this case $Q = 1-a-e_{\Delta s}(\theta)$ is independent on We_r. The condition $Q > 0$ is then equivalent to the condition

$$a < \sqrt[3]{0.25(2+\cos\theta)(1-\cos\theta)^2}. \tag{16}$$

The term under the cubic root is minimum (with value 0) in the limit $\theta \to 0$ and maximum (with value 1) in the limit $\theta \to \pi$. While the condition $\beta_m > 0$ is thus always fulfilled for $a = 0$ (the disc model), it is in the limit $f_w \to 1$ not generally fulfilled for $0 < a \leq 1$. This weakness of the model may be a consequence of approximation (9).

4.1. Ansatz for the dissipation function

So far Eq. (15) is unclosed in f_w. This function should properly describe dissipation in the capillary and viscous regimes. Both asymptotic regimes are commonly distinguished by an impact parameter P, where $P \ll A$ in the capillary regime and $P \gg A$ in the viscous regime with $A > 0$ being of order 1. In literature different relations of the form $P = WeRe^{-b}$ have been proposed with $b = 4/5$ (Clanet et al., 2004), $b = 1/2$ (Fedorchenko et al., 2005) and $b = 2/5$ (Eggers et al., 2010). Recently, Wang et al. (2022) proposed by $P = WeRe^{-4/5}(1-\cos\theta)^2$ an impact parameter that depends on the contact angle.

In selecting an ansatz for the dissipation function f_w we follow an idea from Laan et al. (2014). In their rescaling approach, the authors bridged the dependency of β_m in the capillary and viscous regimes by $\beta_m Re^{-1/5} = P^{1/2}/(A_\beta + P^{1/2})$ where $A_\beta = 1.24$ is a constant obtained by a least-squares fit. Here, we use for the relative dissipation function the ansatz

$$f_w = \frac{P^c}{A + P^c}, \tag{17}$$

where $P = WeRe^{-b}$ and $c > 0$. In the capillary regime ($P^c \ll A$), ansatz (17) yields the scaling $f_w \sim P^c/A$ which results in the inviscid limit $P \to 0$ in $f_w \to 0$. In the viscous regime ($P^c \gg A$), ansatz (17) yields in the limit $P \to \infty$ the result $f_w \to 1$. Appropriate values for the exponents b and c are determined in Section 4.2 while the parameter A is determined in Section 4.3.

4.2. Determination of exponents in impact parameter

The exponents b and c of the impact parameter P are determined by asymptotic analysis assuming $We_r \gg 1$. With parameter a being of order one, the power law scaling of Eq. (15) with respect to We and Re should not be affected by the actual value of a. In this subsection, we use $a = 1$ since this simplifies mathematical expressions. For $We_r \gg 1$ it is $w_\infty \approx We_r$ and

$$Q \approx (1 - f_w)\, We_r = \frac{A}{A + P^c}\, We_r \tag{18}$$

where we used ansatz (17). To study the asymptotic model behaviour, we distinguish two cases depending on the magnitude of the terms in Eq. (15). In the first case, we assume $(Q + \cos\theta)^2 \approx Q^2 + 2Q\cos\theta \gg 4Q(1 - \cos\theta)$ which is equivalent to $Q \gg 4 - 6\cos\theta$. In the second case we assume $Q \ll 4 - 6\cos\theta$ so that $4Q(1 - \cos\theta) \gg (Q + \cos\theta)^2$. Since $Q > 0$ and it is $4 - 6\cos\theta < 0$ for $\theta < 48.2°$, the latter condition can only be fulfilled for superhydrophobic surfaces ($\theta > 150°$).

4.2.1. General case

In the case $Q \gg 4 - 6\cos\theta$ we can approximate Eq. (15) using Eq. (18) and assuming $a = 1$ as

$$\beta_m \approx \sqrt{\frac{4(Q + \cos\theta)}{1 - \cos\theta}} \approx \sqrt{\frac{4Q}{1 - \cos\theta}} \approx \sqrt{\frac{4\, We_r}{1 - \cos\theta} \frac{A}{A + P^c}}. \tag{19}$$

For the inviscid regime where $P^c \ll A$, Eq. (19) yields the approximation $\beta_m \approx \sqrt{4\, We_r/(1 - \cos\theta)} \sim We^{1/2}$. This is the scaling in the large We regime when in absence of dissipation ($Re \to \infty$) initial kinetic energy is converted completely into surface energy at maximum spreading. If a sustained gas film layer develops between the advancing liquid and the substrate as is the case for (skating) free-slip Leidenfrost drops, then Eq. (19) yields for the inviscid case ($P^c \to 0$) in the limit $\theta \to \pi$ the relation $\beta_m \approx \sqrt{We/6}$ (Collings et al., 1990). A scaling $\sim We^{1/2}$ was also derived by Villermaux and Bossa (2011) for the maximum diameter of a radially expanding inviscid liquid sheet using a force/momentum balance.

For $P^c \gg A$ corresponding to the viscous regime, Eq. (19) becomes

$$\beta_m \approx \sqrt{\frac{4A\, We_r P^{-c}}{1 - \cos\theta}} = \sqrt{\frac{A}{3} \frac{We^{1-c} Re^{bc}}{1 - \cos\theta}} \sim We^{(1-c)/2} Re^{bc/2}. \tag{20}$$

The proper choice to ensure the scaling $\beta_m \sim Re^{1/5}$ for the viscous regime is $c = 1$ and $b = 2/5$. This results in $P = WeRe^{-2/5}$, i.e. the impact parameter of Eggers et al. (2010).

It should be noted that the dissipation models $w_m = 3\,WeRe^{-1}\beta_m^4/8$ of Chandra and Avedisian (1991) and $w_m = WeRe^{-0.5}\beta_m^2/3$ of Pasandideh-Fard et al. (1996) both yield the scaling $\beta_m \sim Re^{1/4}$ when $W_m \sim E_{k,0}$ is assumed. To obtain for Eq. (20) the scaling $\beta_m \sim Re^{1/4}$ requires $b = 1/2$ which yields the impact parameter $P = WeRe^{-1/2}$ of Fedorchenko et al. (2005).

4.2.2. Special case relevant for superhydrophobic surfaces only

In the case $Q \ll 4 - 6\cos\theta$ which becomes $Q \ll 10$ in the limit $\theta \to \pi$ we can approximate Eq. (15) using $a = 1$ as

$$\beta_m \approx \sqrt{\frac{2\sqrt{4Q(1-\cos\theta)}}{1-\cos\theta}} \approx \sqrt[4]{\frac{16\,We_r}{1-\cos\theta}\frac{A}{A+P^c}} \approx \sqrt[4]{\frac{8A\,We_r}{A+P^c}} \qquad (21)$$

where we used Eq. (18). For the inviscid regime ($P^c \ll A$), Eq. (21) yields the scaling $\beta_m \sim We^{1/4}$ as observed by Clanet et al. (2004) for the impact of water droplets on a smooth superhydrophobic surface ($\theta_e = 170°$). The same scaling was also observed in experiments on the impact of water drops on a superhydrophobic substrate comprised of hydrophobic micro-pillars, where the liquid spreading is lubricated by an air layer between the drop and the solid surface (Tsai et al., 2011). It should be emphasised that the scaling $\beta_m \sim We^{1/4}$ applies in the limit $\theta \to \pi$ for $Q \ll 10$ only. For $Q \gg 10$ always the scaling $\beta_m \sim We^{1/2}$ of the general case (Section 4.2.1) applies independent on wettability.

By the present analysis, the origin for the two types of Weber number scaling in the capillary regime can be traced back to the quadratic equation for β_m^2 which is obtained from the energy balance when s_m is closed by the approximate spherical cap model with $a > 0$. Depending whether the term that is linear in β_m^2 dominates over the term that is independent on β_m or vice versa, the Weber number scaling $We^{1/2}$ or $We^{1/4}$ is obtained. In general, the Weber number scaling will be $\beta_m \sim We^n$ where $0.25 \leq n \leq 0.5$ according to the two limits as observed e.g. in recent numerical simulations (Wörner et al., 2021).

For the viscous regime ($P^c \gg A$), Eq. (21) yields $\beta_m \approx \sqrt[4]{8A\,We_r P^{-c}} \sim We^{(1-c)/4}Re^{bc/4}$. The proper choice to obtain for the viscous regime the scaling $\beta_m \sim Re^{1/5}$ is $c = 1$ and $b = 4/5$ resulting in $P = WeRe^{-4/5}$, i.e. the

impact parameter of Clanet et al. (2004). Thus, for the cases of Section 4.2.1 and Section 4.2.2, the same exponent value $c = 1$ is obtained for the impact parameter P in the ansatz for the dissipation function, which was not clear a priori. In contrast, for P itself, a different Reynolds number exponent b is obtained for the cases of Section 4.2.1 and Section 4.2.2 to ensure the same scaling $\beta_m \sim Re^{1/5}$ in the viscous regime. This suggests that b could actually be formulated as a function of the contact angle and Q. In the sequel we will use, however, the value $b = 2/5$ determined for the more general case of Section 4.2.1 so that $P = We Re^{-2/5}$.

4.3. Determination of regime discrimination parameter

We now determine parameter A. By definition, f_w is the ratio between dissipation upon maximum spread and dissipation upon terminal state. From division of Eq. (5) by Eq. (11) it follows for this ratio

$$\frac{w_m}{w_\infty} = \frac{1 - a - 0.25\beta_m^4(\beta_m^2 + 4a)^{-1} + 0.25\beta_m^2 \cos\theta + We_r}{1 - \sqrt[3]{0.25(2 + \cos\theta)(1 - \cos\theta)^2} + We_r}, \tag{22}$$

where we used $s_m = s_{\mathrm{asc}}(\beta_m, a)$ and Eq. (14). To obtain for values $\beta > 1$ good agreement of the approximate spherical model with the cylindrical disc model we choose $a = 0.75$. With parameter a fixed, equation (22) enables to estimate values of relative dissipation f_w from experimental data where β_m is measured for certain values of We, Re and θ.

At this stage, it is necessary to specify the characteristic contact angle that shall be used in the present model. The value of the contact angle at the instant in time when the advancing contact line comes to rest at diameter d_m is the advancing contact angle. Therefore, we estimate w_m in the numerator of Eq. (22) using θ_a. The value of the contact angle at the instant in time when the receding contact line comes to rest at the terminal diameter d_∞ is the receding contact angle. Therefore, w_∞ in the denominator of Eq. (22) should be evaluated using $\theta_r = \theta_a - \Delta\theta$. With these determinations, the regime discrimination parameter A becomes a function of the advancing contact angle and of contact angle hysteresis. This setting has the advantage that both θ_a and θ_r are well defined and can, in contrast to θ_e, be measured reproducible with low uncertainty over a wide range of surface wettability (Liu et al., 2019).

Unfortunately, we could find in literature only two references where both the advancing contact angle and contact angle hysteresis are reported for drop

impact experiments measuring β_m. Gao and Li (2014) probe five substrates with different wettability for $We \approx 134$ only. The measurements by Lin et al. (2022) on four different surfaces are more extensive, but are still insufficient to determine $A = A(\theta_a, \Delta\theta)$ from Eq. (22). We therefore resort to other experimental data sets from literature assuming zero contact angle hysteresis ($\Delta\theta = 0$) for now.

Figure 3 displays results for the ratio w_m/w_∞ versus impact parameter $P = WeRe^{-2/5}$ as evaluated for experiments of Aksoy et al. (2022) by Eq. (22). As liquids, seven different water-glycerol mixtures were used, including pure water and pure glycerol. Independent on glycerol concentration, an advancing contact angle $\theta_a = 100°$ is reported. The data set consists of 294 values of β_m measured for Weber and Reynolds numbers in the ranges $57 < We < 460$ and $4 < Re < 9200$. The minimum value of P is about 3 so that the entire data set is in the viscous regime. Largest values of P are obtained for pure glycerol, where $w_m/w_\infty \approx 1$. With decrease of viscosity, P and w_m/w_∞ decrease as well. Figure 3 shows that the experimental data of Aksoy et al. (2022) are well fitted by Eq. (17) using $A = 1.5$

Also included in Fig. 3 are experimental data of Clanet et al. (2004). The authors studied the impact of water droplets on a superhydrophobic surface ($\theta_e = 170°$) for $2.6 < We < 282$. Superhydrophobic surfaces have often very low contact angle hysteresis so that it is reasonable to assume $\theta_a \approx \theta_e$. Since values of Re are not reported in Clanet et al. (2004) but are required to determine P, we additionally assume that the water experiments are all performed with the mentioned diameter $d_0 = 2.5$ mm resulting in the fixed Ohnesorge number $Oh = 0.00236$. With $0.19 < P < 8.1$ the experimental data of Clanet et al. (2004) cover both the capillary and the viscous regime. Associated with the decrease of P is a notable decrease of w_m/w_∞. For the the three lowest values of P relative dissipation upon maximum spread is below 20% of total energy dissipation upon terminal equilibrium. Figure 3 shows that the experimental data of Clanet et al. (2004) are well fitted by ansatz (17) using $A = 2.2$. Thus A depends in a yet unknown manner on the advancing contact angle.

The functional dependence $A = A(\theta_a)$ is determined from Fig. 4 where experimental data of Lee et al. (2016b) are displayed. The authors studied the drop impact of three different liquids (ethanol, water, glycerol) on three different surfaces (glass, steel, parafilm). The ranges of the Weber and Reynolds numbers are $1 < We < 1200$ and $40 < Re < 17\ 800$, respectively. For each liquid-solid combination the authors report the equilibrium

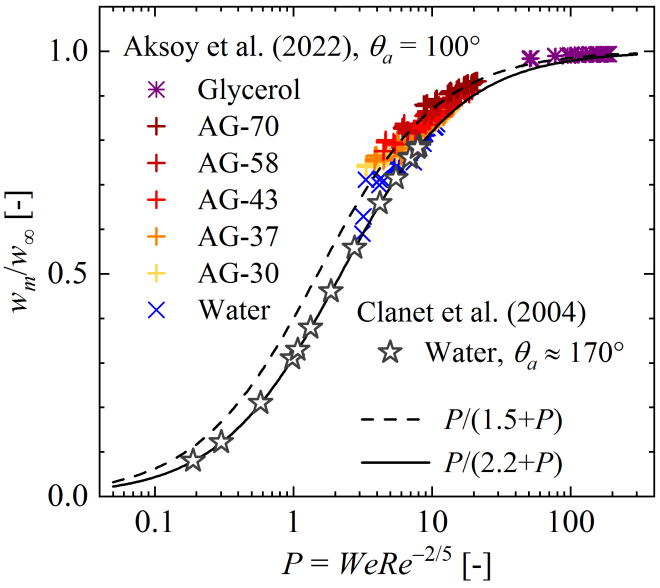

Figure 3: Relative dissipation upon maximum spread versus impact parameter. Symbols: Evaluation of Eq. (22) using experimental data of Aksoy et al. (2022) and Clanet et al. (2004). Lines: fits by Eq. (17) with variable parameter A.

contact angle and the dynamic contact angle where $0° < \theta_e < 110°$ and $44° < \theta_d < 123°$ (see legend in Fig. 4). Here, we assume $\theta_a \approx \theta_d$. From the in total 604 data points of Lee et al. (2016b), four data points for glycerol at low values of P give negative values for w_m/w_∞. Note that due to the lower limit of the y-axis only one of these data points is visible in Fig. 4. The nonphysical result of negative values for w_m indicates that assuming zero contact angle hysteresis may be not appropriate here.

From Fig. 3 and Fig. 4 the parameter A in ansatz (17) is determined as $A(\theta_a) = 1.2 - \cos\theta_a$. In the limit $\theta_a \to 0$ it is thus $A = 0.2$ while for $\theta_a \to \pi$ it is $A = 2.2$. The final form of the dissipation function $f_w = f_w(We, Re, \theta_a)$ is then obtained as

$$f_w = \frac{WeRe^{-2/5}}{1.2 - \cos\theta_a + WeRe^{-2/5}}. \tag{23}$$

In contrast to Wang et al. (2022), who proposed an impact parameter that depends on the contact angle, the impact parameter in the present model is independent on contact angle. Instead, the parameter A that discriminates

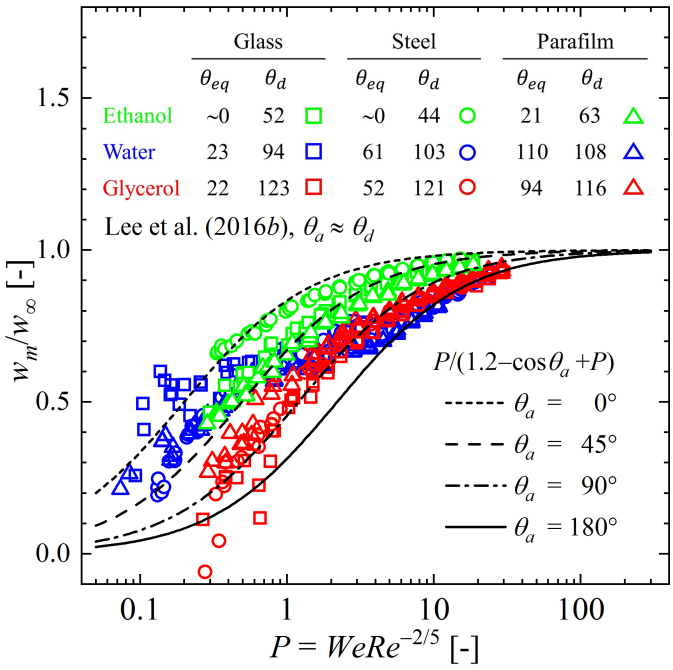

Figure 4: Relative dissipation upon maximum spread versus impact parameter. Symbols: Evaluation of Eq. (22) using experimental data of Lee et al. (2016b) assuming $\theta_a \approx \theta_d$. Lines: fits by Eq. (17) with $A = 1.2 - \cos\theta_a$ for four different values of θ_a.

the capillary and viscous regimes is shown (by analysis of experimental results) to depend on the (advancing) contact angle.

Relation (23) for the relative dissipation at maximum spread is obtained from evaluation of experimental data. This relation suggests that for fixed P liquid repellent surfaces ($\cos\theta_a < 0$) dissipate less energy upon maximum spread as compared to liquid attracting surfaces ($\cos\theta_a > 0$). This reflects why after recoil from maximum spread only droplets impinging on surfaces with reduced wettability (large θ) may possess sufficient excess energy to enable bounce back (Fink et al., 2018).

Exponents in the dissipation function (23) have been derived from asymptotic relations assuming $We_r \gg 1$. For zero impact velocity it is $We = 0$. Eq. (23) then yields $f_w = 0$, thus predicting zero dissipation at maximum spread for zero impact velocity, similar to other dissipation models in literature. For $We = 0$, the total dissipation is $w_\infty = e_{\Delta s}$, cf. Eq. (14). The difference between normalised initial and terminal surface energy $e_{\Delta s}$ is pos-

itive for $\theta \in (0, \pi)$. This implies that with the present model the excess surface energy is dissipated completely during the recoil process, which is not realistic. Furthermore, for $We = f_w = 0$ it is $Q = 1 - a$ and Eq. (15) yields a relation for β_m that depends on parameter a only. This is a further weakness of the present model. It is related to the modelling of drop shape at maximum spread as approximate spherical cap while the terminal drop shape is considered as exact spherical cap, cf. the discussion of Eq. (16).

4.4. Model performance

Aksoy et al. (2022) used their experimental data set to test the performance of four spreading models from literature derived from an energy balance. The models of Pasandideh-Fard et al. (1996) and Ukiwe and Kwok (2005) strongly underestimate the spreading of pure glycerol and are found unsuited for high viscous liquids. The models of Chandra and Avedisian (1991) and Du et al. (2021) predict the data set of Aksoy et al. (2022) with an accuracy of about 30% and 20%, respectively. The model of Aksoy et al. (2022) developed based on their own experiments yields an accuracy of about 10%, which reduces to about 30% for other experimental data sets from literature. Lee et al. (2016b) compare in Fig. 6 of their paper their experimental data with the rescaling model for β_m developed by the authors. The ordinate in that figure has, however, no labels. Since the accuracy of the rescaling model is also not mentioned in the text, the deviation between data and model in Lee et al. (2016b) is unclear.

The model proposed in this paper is given by equation (15), where $\theta = \theta_a$ and $a = 0.75$, with Q, w_∞ and f_w as defined in equations (13), (14) and (23), respectively. Fig. 5 illustrates the performance of the proposed model against the three experimental data sets underlying its development (Clanet et al., 2004; Lee et al., 2016b; Aksoy et al., 2022) by a parity plot. The large variation of surface wettability ($0° < \theta_e < 170°$) and liquid viscosity ($1 - 1021$ mPa s) in the experiments results in wide variations of Weber number ($1 - 1200$), Reynolds number ($4 - 17\,800$), impact parameter ($0.07 - 188$) and maximum spread factor β_m ($1.2 - 5.6$). For each individual experimental data point the value of Q is positive and within the range $0.15 < Q < 5.8$ for the entire data set. This indicates the consistency and robustness of the present model, as for some data of Lee et al. (2016b) negative values of f_w are obtained.

The main diagram of Fig. 5 shows that with exception of the ethanol data for steel of Lee et al. (2016b) all data form one consistent band. In general,

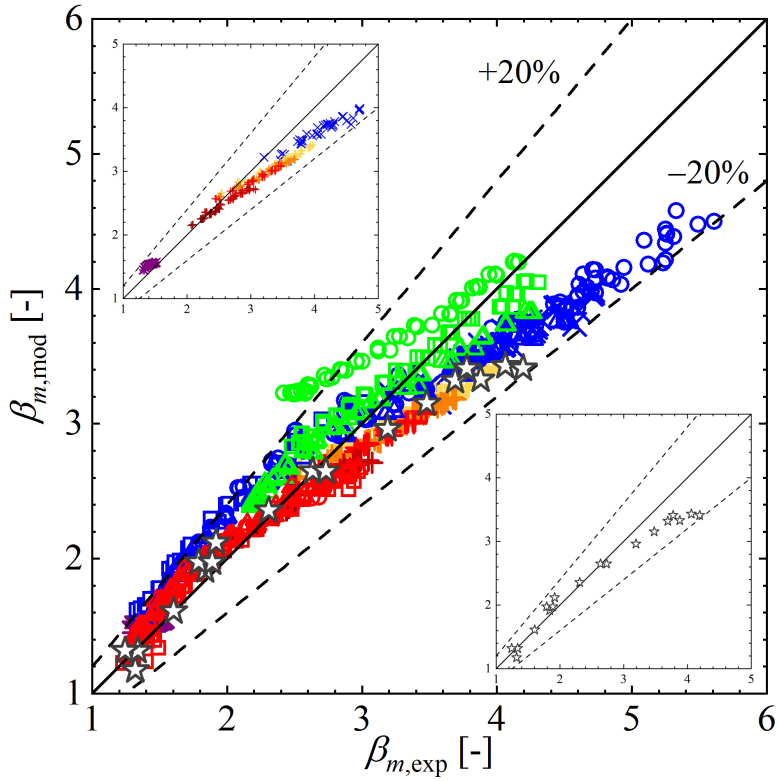

Figure 5: Parity plot of β_m comparing model predictions with experiments by Aksoy et al. (2022) (main diagram and upper left inset), Clanet et al. (2004) (main diagram and lower right inset) and Lee et al. (2016b) (main diagram). Dashed lines in the main diagram and both insets indicate a deviation by ±20%. For legends to the various symbols see Fig. 3 and Fig. 4.

the proposed model tends to overestimate the experimental data for $\beta_m < 3$ and to underestimate them for $\beta_m > 3$. The reasons for these systematic deviations are unclear. A possible cause could be that kinetic energy at maximum spreading is neglected in the model. With a maximum deviation of ±20% the overall agreement of the present model with all experimental data is reasonable good given the wide ranges of We, Re and wettability.

5. Conclusions

Based on an energy balance approach a new explicit model for the maximum spread factor (β_m) during axi-symmetric drop impact on a dry surface

in absence of splashing is developed. Normalised gas-liquid surface area at maximum spread (s_m) is modelled by an approximation derived from an analytical expression valid for a spherical cap. Normalised accumulative dissipation upon maximum spread (w_m) is modelled relative to the upper physical bound for normalised dissipation (w_∞). The latter is determined from a second energy balance for the terminal state when the drop is at rest possessing only gas-liquid surface energy according to its terminal shape, which is modelled as spherical cap.

Relative dissipation $f_w = w_m/w_\infty$ is modelled as function of the impact parameter $P = WeRe^{-2/5}$ and a regime discrimination parameter A allowing for a smooth transition between the scaling in the capillary and viscous regimes. Exponents of the Weber number and the Reynolds number in the impact parameter are determined by asymptotic analysis. Thereby the model is the first one that includes the power law scaling of the viscous regime where $\beta_m \sim Re^{1/5}$ and that of two distinct capillary regimes where either $\beta_m \sim We^{1/2}$ or $\beta_m \sim We^{1/4}$, respectively. It is shown that the scaling $\beta_m \sim We^{1/4}$ applies to superhydrophobic surfaces under certain conditions only. It is argued that the regime discrimination parameter A should be formulated as function of the advancing contact angle (θ_a) and of contact angle hysteresis ($\Delta\theta$). Since information on contact angle hysteresis in drop impact experiments is missing in literature, the relation $A(\theta_a) = 1.2 - \cos\theta_a$ is determined by analysis of experimental spreading data from literature neglecting any possible dependence on contact angle hysteresis so far.

It is believed that the proposed modelling approach constitutes a physically sound basis for development of a real universal mechanistic energy balance model for predicting maximum spread during drop impact. The accuracy of the proposed model in comparison to experimental data by Clanet et al. (2004), Lee et al. (2016b) and Aksoy et al. (2022) is about 20%. For further improvement, the model should be tested against more experimental or numerical data sets. Model refinement should focus on the regime discrimination parameter A, which should be formulated in addition to θ_a as function of contact angle hysteresis. For this purpose new experimental data are required. Further generalisations are the consideration of a non-zero kinetic energy at maximum spread and the inclusion of gravitational energy in the energy balance. Both extensions may affect the modelling of $A(\theta_a, \Delta\theta)$.

Acknowledgement. The author thanks Y.T. Aksoy and J.B. Lee for providing files with their original experimental data.

Funding. German Research Foundation (DFG), project 237267381 - TRR 150, subproject B08.

Declaration of Interests. The author reports no conflict of interest.

Appendix A. Derivation of Eq. (8)

The area of the curved surface of a spherical cap with base radius r and height h is

$$S_{sc} = \pi(h^2 + r^2). \tag{A.1}$$

The volume of the spherical cap is

$$V_{sc} = \frac{\pi}{6}h(3r^2 + h^2) = \frac{\pi}{6}d_0^3, \tag{A.2}$$

where d_0 denotes the diameter of a spherical drop with the same volume. By taking the square of Eq. (A.2) it follows

$$h^2(3r^2 + h^2)^2 = d_0^6. \tag{A.3}$$

Eliminating h^2 from Eq. (A.3) by using Eq. (A.1) and introducing the notations $s_{sc} = S_{sc}/(\pi d_0^2)$ and $\beta = 2r/d_0$ yields

$$s_{sc}^3 + \frac{3}{4}\beta^2 s_{sc}^2 - \frac{1}{16}\beta^6 - 1 = 0. \tag{A.4}$$

This cubic equation in s_{sc} has one real solution as given by Eq. (8).

References

Aksoy, Y.T., Eneren, P., Koos, E., Vetrano, M.R., 2022. Spreading of a droplet impacting on a smooth flat surface: how liquid viscosity influences the maximum spreading time and spreading ratio. Phys. Fluids 34, 042106. doi:10.1063/5.0086050.

Almohammadi, H., Amirfazli, A., 2019. Droplet impact: Viscosity and wettability effects on splashing. Journal of Colloid and Interface Science 553, 22–30. doi:10.1016/j.jcis.2019.05.101.

Asai, A., Shioya, M., Hirasawa, S., Okazaki, T., 1993. Impact of an ink drop on paper. Journal of Imaging Science and Technology 37, 205–207.

Attané, P., Girard, F., Morin, V., 2007. An energy balance approach of the dynamics of drop impact on a solid surface. Phys. Fluids 19, 012101. doi:10.1063/1.2408495.

Bayer, I.S., Megaridis, C.M., 2006. Contact angle dynamics in droplets impacting on flat surfaces with different wetting characteristics. J. Fluid Mech. 558, 415–449. doi:10.1017/S0022112006000231.

Bennett, T., Poulikakos, D., 1993. Splat-quench solidification: Estimating the maximum spreading of a droplet impacting a solid-surface. J. Mater. Sci. 28, 963–970. doi:10.1007/Bf00400880.

Breitenbach, J., Roisman, I.V., Tropea, C., 2018. From drop impact physics to spray cooling models: A critical review. Exp.Fluids 59, 55. doi:10.1007/s00348-018-2514-3.

Budakli, M., 2021. Prediction of maximum spreading factor after drop impact: Development of a novel semi-analytical model incorporating effect of surface roughness. Colloid Interface Sci. Commun. 41, 100384. doi:10.1016/j.colcom.2021.100384.

Butt, H.J., Liu, J., Koynov, K., Straub, B., Hinduja, C., Roisman, I.V., Berger, R., Li, X., Vollmer, D., Steffen, W., Kappl, M., 2022. Contact angle hysteresis. Curr. Opin. Colloid Interface Sci. 59, 101574. doi:10.1016/j.cocis.2022.101574.

Castrejon-Pita, J.R., Baxter, W.R.S., Morgan, J., Temple, S., Martin, G.D., Hutchings, I.M., 2013. Future, opportunities and challenges of inkjet technologies. Atomiz. Sprays 23, 541–565. doi:10.1615/AtomizSpr.2013007653.

Chandra, S., Avedisian, C.T., 1991. On the collision of a droplet with a solid surface. Proc. R. Soc. Lond. A 432, 13–41. doi:10.1098/rspa.1991.0002.

Clanet, C., Béguin, C., Richard, D., Quéré, D., 2004. Maximal deformation of an impacting drop. J. Fluid Mech. 517, 199–208. doi:10.1017/S0022112004000904.

Collings, E.W., Markworth, A.J., McCoy, J.K., Saunders, J.H., 1990. Splat-quench solidification of freely falling liquid-metal drops by impact on a planar substrate. J. Mater. Sci. 25, 3677–3682. doi:10.1007/BF00575404.

Cox, R.G., 1986. The dynamics of the spreading of liquids on a solid-surface. part 1. viscous-flow. J. Fluid Mech. 168, 169–194. doi:10.1017/S0022112086000332.

Du, J., Wang, X., Li, Y., Min, Q., Wu, X., 2021. Analytical consideration for the maximum spreading factor of liquid droplet impact on a smooth solid surface. Langmuir 37, 7582–7590. doi:10.1021/acs.langmuir.1c01076.

Eggers, J., Fontelos, M.A., Josserand, C., Zaleski, S., 2010. Drop dynamics after impact on a solid wall: Theory and simulations. Phys. Fluids 22, 062101. doi:10.1063/1.3432498.

Engel, O.G., 1955. Waterdrop collisions with solid surfaces. J. Res. Nat. Bur. Stand. 54, 281–298. doi:10.6028/jres.054.033.

Fang, W., Zhang, K., Jiang, Q., Lv, C., Sun, C., Li, Q., Song, Y., Feng, X.Q., 2022. Drop impact dynamics on solid surfaces. Appl. Phys. Lett. 121, 210501. doi:10.1063/5.0124256.

Fedorchenko, A.I., Wang, A.B., Wang, Y.H., 2005. Effect of capillary and viscous forces on spreading of a liquid drop impinging on a solid surface. Phys. Fluids 17, 093104. doi:10.1063/1.2038367.

Fink, V., Cai, X., Stroh, A., Bernard, R., Kriegseis, J., Frohnapfel, B., Marschall, H., Wörner, M., 2018. Drop bouncing by micro-grooves. Int. J. Heat Fluid Flow 70, 271–278. doi:10.1016/j.ijheatfluidflow.2018.02.014.

Ford, R.E., Furmidge, C.G.L., 1967. Impact and spreading of spray drops on foliar surfaces. Wetting (Soc. Chem. Ind. Mongraph.) 25, 417–432.

Gao, X., Li, R., 2014. Spread and recoiling of liquid droplets impacting solid surfaces. AIChE J. 60, 2683–2691. doi:10.1002/aic.14440.

de Gennes, P.G., 1985. Wetting: Statics and dynamics. Rev. Mod. Phys. 57, 827–863. doi:10.1103/RevModPhys.57.827.

German, G., Bertola, V., 2009. Review of drop impact models and validation with high-viscosity Newtonian fluids. Atomiz. Sprays 19, 787–807. doi:10.1615/AtomizSpr.v19.i8.60.

Gordillo, J.M., Riboux, G., Quintero, E.S., 2019. A theory on the spreading of impacting droplets. J. Fluid Mech. 866, 298–315. doi:10.1017/jfm.2019.117.

Josserand, C., Thoroddsen, S., 2016. Drop impact on a solid surface. Annu. Rev. Fluid Mech. 48, 365–391. doi:10.1146/annurev-fluid-122414-034401.

Kim, H.Y., Chun, J.H., 2001. The recoiling of liquid droplets upon collision with solid surfaces. Phys. Fluids 13, 643–659. doi:10.1063/1.1344183.

Kung, C.H., Sow, P.K., Zahiri, B., Mérida, W., 2019. Assessment and interpretation of surface wettability based on sessile droplet contact angle measurement: Challenges and opportunities. Adv. Mater. Interfaces 6, 1900839. doi:10.1002/admi.201900839.

Laan, N., de Bruin, K.G., Bartolo, D., Josserand, C., Bonn, D., 2014. Maximum diameter of impacting liquid droplets. Phys. Rev. Appl. 2. doi:10.1103/PhysRevApplied.2.044018.

Lee, J.B., Derome, D., Dolatabadi, A., Carmeliet, J., 2016a. Energy budget of liquid drop impact at maximum spreading: Numerical simulations and experiments. Langmuir 32, 1279–1288. doi:10.1021/acs.langmuir.5b03848.

Lee, J.B., Laan, N., de Bruin, K.G., Skantzaris, G., Shahidzadeh, N., Derome, D., Carmeliet, J., Bonn, D., 2016b. Universal rescaling of drop impact on smooth and rough surfaces. J. Fluid Mech. 786, R4. doi:10.1017/jfm.2015.620.

Li, R., Ashgriz, N., Chandra, S., 2010. Maximum spread of droplet on solid surface: Low Reynolds and Weber numbers. J. Fluids Eng. 132, 061302. doi:10.1115/1.4001695.

Liang, G., Chen, Y., Chen, L., Shen, S., 2019. Maximum spreading for liquid drop impacting on solid surface. Ind. Eng. Chem. Res. 58, 10053–10063. doi:10.1021/acs.iecr.9b02014.

Liang, G., Mudawar, I., 2017. Review of drop impact on heated walls. Int. J. Heat Mass Transfer 106, 103–126. doi:10.1016/j.ijheatmasstransfer.2016.10.031.

Lin, S., Wang, Y., Sun, L., Mehrizi, A.A., Jin, Y., Chen, L., 2022. Experimental and numerical investigations on the spreading dynamics of impinging liquid droplets on diverse wettable surfaces. Int. J. Multiph. Flow 153, 104135. doi:10.1016/j.ijmultiphaseflow.2022.104135.

Liu, K., Vuckovac, M., Latikka, M., Huhtamäki, T., Ras, R.H.A., 2019. Improving surface-wetting characterization. Science 363, 1147–1148. doi:10.1126/science.aav5388.

Madejski, J., 1976. Solidification of droplets on a cold surface. Int. J. Heat Mass Transfer 19, 1009–1013. doi:10.1016/0017-9310(76)90183-6.

Mao, T., Kuhn, D.C.S., Tran, H., 1997. Spread and rebound of liquid droplets upon impact on flat surfaces. AIChE J. 43, 2169–2179. doi:10.1002/aic.690430903.

Marengo, M., Antonini, C., Roisman, I.V., Tropea, C., 2011. Drop collisions with simple and complex surfaces. Curr. Opin. Colloid Interface Sci. 16, 292–302. doi:10.1016/j.cocis.2011.06.009.

Marmur, A., Della Volpe, C., Siboni, S., Amirfazli, A., Drelich, J.W., 2017. Contact angles and wettability: Towards common and accurate terminology. Surf. Innov. 5, 3–8. doi:10.1680/jsuin.17.00002.

Moreira, A.L.N., Moita, A.S., Panão, M.R., 2010. Advances and challenges in explaining fuel spray impingement: How much of single droplet impact research is useful? Prog. Energy Combust. Sci. 36, 554–580. doi:10.1016/j.pecs.2010.01.002.

Park, H., Carr, W.W., Zhu, J., Morris, J.F., 2003. Single drop impaction on a solid surface. AIChE J. 49, 2461–2471. doi:10.1002/aic.690491003.

Pasandideh-Fard, M., Qiao, Y.M., Chandra, S., Mostaghimi, J., 1996. Capillary effects during droplet impact on a solid surface. Phys. Fluids 8, 650–659. doi:10.1063/1.868850.

Qin, M., Tang, C., Tong, S., Zhang, P., Huang, Z., 2019. On the role of liquid viscosity in affecting droplet spreading on a smooth solid surface. Int. J. Multiph. Flow 117, 53–63. doi:10.1016/j.ijmultiphaseflow.2019.05.002.

Rein, M., 1993. Phenomena of liquid drop impact on solid and liquid surfaces. Fluid Dyn. Res. 12, 61. doi:10.1016/0169-5983(93)90106-K.

Renardy, Y., Popinet, S., Duchemin, L., Renardy, M., Zaleski, S., Josserand, C., Drumright-Clarke, M.A., Richard, D., Clanet, C., Quéré, D., 2003. Pyramidal and toroidal water drops after impact on a solid surface. J. Fluid Mech. 484, 69–83. doi:10.1017/S0022112003004142.

Roisman, I.V., 2009. Inertia dominated drop collisions. II. An analytical solution of the Navier–Stokes equations for a spreading viscous film. Phys. Fluids 21, 052104. doi:10.1063/1.3129283.

Roisman, I.V., Rioboo, R., Tropea, C., 2002. Normal impact of a liquid drop on a dry surface: Model for spreading and receding. Proc. R. Soc. Lond. A 458, 1411–1430. doi:10.1098/rspa.2001.0923.

Samkhaniani, N., Stroh, A., Holzinger, M., Marschall, H., Frohnapfel, B., Wörner, M., 2021. Bouncing drop impingement on heated hydrophobic surfaces. Int. J. Heat Mass Transfer 180, 121777. doi:10.1016/j.ijheatmasstransfer.2021.121777.

Scheller, B.L., Bousfield, D.W., 1995. Newtonian drop impact with a solid surface. AIChE J. 41, 1357–1367. doi:10.1002/aic.690410602.

Tsai, P., Hendrix, M.H.W., Dijkstra, R.R.M., Shui, L., Lohse, D., 2011. Microscopic structure influencing macroscopic splash at high Weber number. Soft Matter 7, 11325–11333. doi:10.1039/c1sm05801k.

Ukiwe, C., Kwok, D.Y., 2005. On the maximum spreading diameter of impacting droplets on well-prepared solid surfaces. Langmuir 21, 666–673. doi:10.1021/la0481288.

Vadillo, D.C., Soucemarianadin, A., Delattre, C., Roux, D.C.D., 2009. Dynamic contact angle effects onto the maximum drop impact spreading on solid surfaces. Phys. Fluids 21, 122002. doi:10.1063/1.3276259.

Villermaux, E., Bossa, B., 2011. Drop fragmentation on impact. J. Fluid Mech. 668, 412–435. doi:10.1017/S002211201000474x.

Voinov, O., 1976. Hydrodynamics of wetting. Fluid Dynamics 11, 714–721. doi:10.1007/BF01012963.

Wang, F., Yang, L., Wang, L., Zhu, Y., Fang, T., 2019. Maximum spread of droplet impacting onto solid surfaces with different wettabilities: Adopting a rim-lamella shape. Langmuir 35, 3204–3214. doi:10.1021/acs.langmuir.8b03748.

Wang, R., Shi, Y.Z., Zhang, C.Y., Ding, H., 2022. On the maximal spreading of drops impacting onto a no-slip substrate. Phys. Fluids 34, 052103. doi:10.1063/5.0089619.

Wildeman, S., Visser, C.W., Sun, C., Lohse, D., 2016. On the spreading of impacting drops. J. Fluid Mech. 805, 636–655. doi:10.1017/jfm.2016.584.

Willis, K., Orme, M., 2003. Binary droplet collisions in a vacuum environment: An experimental investigation of the role of viscosity. Exp. Fluids 34, 28–41. doi:10.1007/s00348-002-0526-4.

Wörner, M., Samkhaniani, N., Cai, X., Wu, Y., Majumdar, A., Marschall, H., Frohnapfel, B., Deutschmann, O., 2021. Spreading and rebound dynamics of sub-millimetre urea-water-solution droplets impinging on substrates of varying wettability. Appl. Math. Mod. 95, 53–73. doi:10.1016/j.apm.2021.01.038.

Yarin, A.L., 2006. Drop impact dynamics: Splashing, spreading, receding, bouncing... Annu. Rev. Fluid Mech. 38, 159–192. doi:10.1146/annurev.fluid.38.050304.092144.

Ye, Q., Domnick, J., 2017. Analysis of droplet impingement of different atomizers used in spray coating processes. J. Coat. Technol. Res. 14, 467–476. doi:10.1007/s11998-016-9867-4.

Yonemoto, Y., Kunugi, T., 2017. Analytical consideration of liquid droplet impingement on solid surfaces. Sci. Rep. 7, 2362. doi:10.1038/s41598-017-02450-4.

Zhang, X., Ji, B., Liu, X., Ding, S., Wu, X., Min, J., 2021. Maximum spreading and energy analysis of ellipsoidal impact droplets. Phys. Fluids 33, 052108. doi:10.1063/5.0047583.

Zhang, Z., Zhang, P., 2019. Numerical interpretation to the roles of liquid viscosity in droplet spreading at small Weber numbers. Langmuir 35, 16164–16171. doi:10.1021/acs.langmuir.9b02736.